

Original Research

Dust Release during Playa Activation in a Typical Semiarid Steppe

Shuai Qi¹, Xiaomeng Ren², Zhongju Meng^{1*}, Xiaohong Dang¹,
Haonian Li¹, Ruiting Jia³

¹College of Desert Control Science and Engineering, Inner Mongolia Agricultural University, Hohhot 010018, China

²Inner Mongolia Meteorological Institute, Hohhot 010051, China

³Inner Mongolia Academy of Forestry, Hohhot, 010010, China

Received: 16 August 2022

Accepted: 9 November 2022

Abstract

Playas are one of the major sources of saline and alkaline dust in northern China, which release a large amount of sand and dust material every year, severely impacting the quality of the atmosphere, production and life on the Inner Mongolian Plateau in northern China. The surface characteristics of playa activation processes influence the horizontal salt migration flux, but the salt transmission volume of playas is almost unknown in dry salt lakes in a typical steppe. The functional relationship between horizontal salt dust transmission volume and the grain size content was ascertained for four different surfaces at situ sites in the Chagan Nur playa in northern China. After collecting salt dust from four surfaces (crust, broken crust, activated and sandy saline surface) formed during different stages of the desiccation process, the salt dust transmission was assessed based on the wind velocity profile, grain size, and total wind erosion particulate matter (TWEP) profiles above the playa surfaces. The particle size gradually increased from the center of the lake to the shore, while the water content decreased. The wind speed, friction velocity, and roughness of the four surfaces were as follows: sandy saline surface < crust surface < broken crust surface < activated surface. The sand transport of crust in the height range of up to 50 cm was a linear function of the sand transport rate, while the sand transport of the broken crust obeyed a power function, and the activated and sandy saline surfaces obeyed an exponential function. The formation of a stable crust surface by fine particles reduced the wind erosion of the playa, but the playa was still a potentially huge source of salt dust during and after activation and the dust generated by the activated surface (2.61 g/cm²·min) was 20 times that generated from the crust cover (0.13 g/cm²·min) during the observation period. Finally, all of the aerosol substances were <63 μm.

Keywords: typical steppe playa, wind erosion, sediment transport, salt crust, particle size

*e-mail: mengzhongju@126.com

Introduction

The drying up of lakes is a significant problem in arid and semiarid areas which leads to the exposure of fine-grained lacustrine sediments at the surface, increasing the salinity of the land, decreasing the soil productivity, forming saline desertification, and increasing the risk of regional wind erosion, and generating chemical dust storms [1]. To explore the main global dust sources, Varga et al. [2, 3] used satellite images from the Total Ozone Mapping Spectrometer acquired from 1979 to 2011, confirming that playas and dry rivers in arid and semi-arid regions were one of the main dust sources. Furthermore, Middleton et al. [4, 5] have also proven that dried up lakes and beaches were considered to be the major dust sources in the world. The Xilingol Plateau is a landscape unit with multiple types of grassland, sandy land, and lakes, and it extends across of the Inner Mongolian Plateau in northern China. The playa cover on the Xilingol Plateau is mainly derived from grassland degradation, and a large number of fine salt materials have formed loose sediment particles after the lakes dried up. In recent years, due to drastic climate change and irrational human exploitation, a large number of lakes have shrunk and become new sources of dust in semi-arid areas, which is an important issue [6]. The East Asian summer monsoon is one active and important component of the global climate system, which transports moisture vapor and heat from southeastern India and the western Pacific to northern Asia [7]. The changeable climate of the East Asian winter monsoon system is also one of the active components of the global climate system, and it affects the temperature in both nearby areas and northern China. It has a great impact on the semiarid areas of the Xilinguole Plateau during spring [8].

The Chagan Nur banner (in the southern part of the Inner Mongolian Plateau), which consists of playas, sandy deserts (the Otindag Sandy Land), and typical temperate steppes, is located on the fringe of the modern East Asian summer-monsoon and East Asian winter -monsoon dominated areas. Chagan Nur Lake is an ecologically fragile area and is extremely sensitive to the changing monsoon climate. The depth of the lake was 7.2 m in the 1950s. The west Chagan Nur Lake completely dried up in 2001 and formed a huge playa, and the water depth of east Chagan Nur lake is only 2.5 m at present [9]. During spring and winter, the Chagan Nur playa is influenced by dry and cold air from Mongolia. Especially in spring, the temperature is above zero degrees during the day and below zero degrees at night, and the freeze-thaw alternation loosens the soil. Both the natural underlying surface of the playa and the changeable climate have caused this playa to become a potential salt dust source area [3]. The soil salt particle size of the playa surface is one of the significant factors influencing wind erosion, and PM₁₀, PM_{2.5}, and other dust emissions. Alizadeh et al. [3, 10] proved that the soil clay content affects

the adhesion of the soil particles, the clay content contributes to the formation of an aggregate structure, and the size of soil particles determines the surface tension and cohesion of the soil, making it an important parameter affecting soil wind erosion. During the wind erosion process, the minimum wind speed required for the soil to overcome the resistance (resistance to movement due to the gravity of particles and cohesion between particles) is the threshold friction speed. Soil salt particles not only affect the friction speed of the playa but also affect the number of dust emissions and the delivery distance [11].

Since Chagan Nur Lake dried up, the frequency of sandstorms in Chagan playa and nearby cities has increased. However, the lack of dust emission monitoring around Chagan Nur Lake, has resulted in the limited availability of dust supply information for Chagan playa during wind erosion events. According to our previous investigation, there has been no field monitoring of the characteristics of the wind erosion of this dry lake in a typical semi-arid steppe or its emission characteristics during wind erosion. Therefore, Chagan Nur playa was chosen to study the release characteristics of salt dust and the transport characteristics of salt dust particles during the drying and activation of the playa.

Materials and Methods

Study Area

The study area is located in Inner Mongolia, northern China (114°45'–115°04'E and 43°22'–43°29'N). The climate is semiarid with a mean annual precipitation of 240 mm, 90% of which occurs from June to September. The evaporation is about 2000 mm, and the average annual temperature is 0.6°C, with a minimum temperature of -42.4°C and a maximum temperature of 39.1°C. The average wind speed at a height of 2 m is 3.5 m/s, and the maximum wind speed is 22.6 m/s. The direction of the wind changes mainly in 3 directions (northwest, west, and north), with the most severe wind erosion occurring in spring. The main plants in the study area are *Tamarix*, *Haloxylon*, *Suaeda corniculata*, and *Achnatherum splendens*. Due to the low vegetation coverage and loose soil in the study area and the frequent high wind events, wind erosion of the playa often occurs.

Sampling Site Selection and Experimental Design

There was a region without any vegetation in the northwestern corner of west Chagan Nur Lake. According to information obtained from herders, it was protected by planting *Suaeda corniculata* in 2010; then, all of the *Suaeda corniculata* died without any further protection. The activation level of the playa was reconstructed based on the surface morphology,

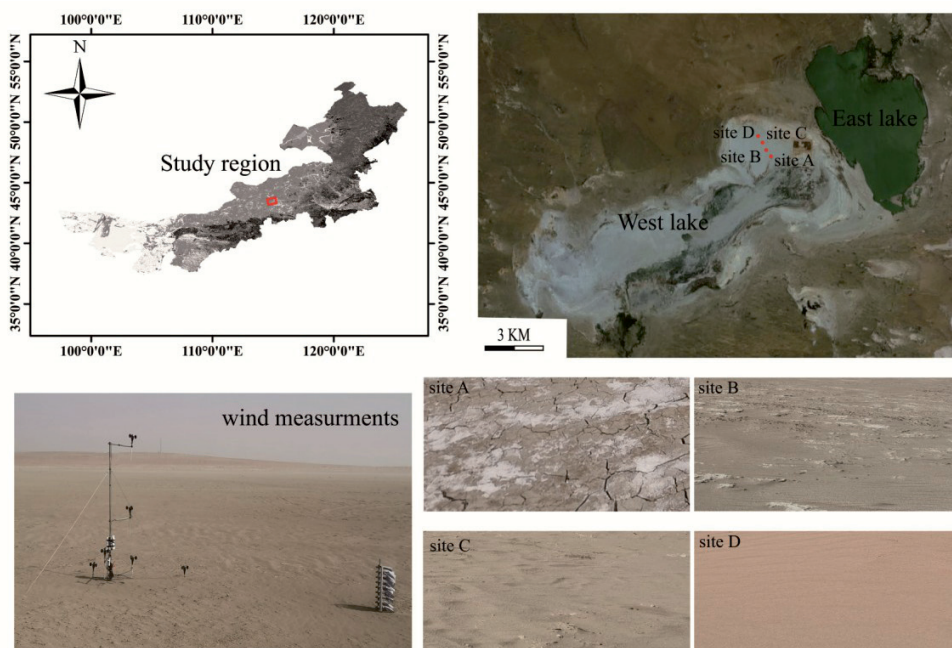


Fig. 1. Study Area Location.

and the distance from the lake center of the lake to the shore increased during the drying process. The exposed location selected in this study was about 2 km long from south to north, and 1 km wide from east to west (Fig. 1). From March to May, the study area received little precipitation, was extremely dry, and had no vegetation coverage, and thus, the most intense wind erosion occurred during this period. Therefore, five high wind events were chosen for field observations during the period from 25 March to 1 May 2021, four representative soil types (A with crust, B with broken crust surface after evaporation and weathering, C with a fully activated surface, D with an activated surface containing sand) were selected with a relative distance of 200 m between any two sites, and all of the sites were located on the playa landform.

Soil Sampling and Analytical Methods

When monitoring the wind erosion events in the area, first, we sampled the surface soils before the wind erosion event, using a small shovel to collect about 100 g of soil from depths up to 2 cm from the ground surface at different locations in the four sampling sites. The soil sample was placed in an aluminum box to determine the soil moisture (%) using the drying method, and 50 g of the soil sample was used to determine the soil's mechanical composition. The hardness of the ground surface was measured five times using a hand-held manometer, and the average value of the sample sites was used. The basic conditions of the ground surface were also recorded.

The horizontal sediment mass flux from wind erosion was measured at the four sampling sites using

a homemade step sand collector (50 cm). The size of each layer was 2 cm × 2 cm, and there were total of 25 layers in each collector. The wind speed was measured using three-cup anemometer at the heights of 0.1, 0.3, 0.5, 1.0, and 2.0 m at the four sampling sites, and the duration of the observation was up to 60 minutes.

Data Processing

1. soil moisture (%)

$$SM = \frac{m_1 - m_2}{m_2 - m} \times 100\% \tag{1}$$

where SM is the soil moisture (%), m_1 is the weight (g) of the aluminum box and wet soil, m_2 is the weight (g) of the aluminum box and dry soil, and m is the weight (g) of the aluminum box.

2. Wind profiles

The wind speed profiles of the four observation sites were expressed using the von Karman-Prandtl equation [12], and the roughness length (Z_0) and friction velocity (U^*) were fitted according to the wind speed profiles using the least squares method [13, 14].

$$U_z = \frac{U^*}{K} \ln \frac{Z}{Z_0} \tag{2}$$

$$U_z = a + b \ln Z \tag{3}$$

$$Z_0 = \exp(-a/b) \tag{4}$$

$$U^* = Kb \quad (5)$$

where U_z is the velocity at height z (m/s); Z_0 is the aerodynamic roughness (m); K is the von Karman's constant (0.4); Z is the measurement height (m); a and b are the regression coefficients; and U^* is the shear velocity (m/s).

3. Sediment transport

Mathematical models of the horizontal sediment flux were used to reflect the sand transport fluxes from the different surfaces. These models mainly focused on linear functions, exponential functions, power functions, and polynomial functions.

$$Q = aH + b \quad (6)$$

$$Q = ae^{-bH} \quad (7)$$

$$Q = aH^{-b} \quad (8)$$

where Q is the amount of sand transported in a certain height layer ($\text{g}/\text{cm}^2\cdot\text{min}^{-1}$); H is the height (cm); and a and b are the wind and sand circulation coefficients.

4. Soil particle size parameters

This experiment was completed in the Wind and Sand Physics Laboratory of the Inner Mongolia Agricultural University. The particle size samples collected were analyzed using a Mastersizer-2100 laser particle size analyzer (0.02-2100 μm) manufactured by RITSCH, Germany. The measurement results were obtained using the Folk-Ward particle size formula and the GRA-DISTAT particle size analysis software for each particle size parameter [15, 16].

Results

Basic Characteristics of the Land Surface

The soil textures of the four sites differed from each other. Site A consisted of a crust with a high water content of 19%. The crust was composed of 52.59% clay, and 47.41% silt, and no sand grains and had the hardest soil surface (3.38 kg/cm^2 to rupture). Site B consisted of 63.81% clay and 31.35% silt, and a small number of sand grains (4.84%). The surface was a crust broken by weathering, and the hardness of the surface 1.69 kg/cm^2 . Site C consisted of 57.08% clay, 42.61% silt and only 0.31% sand. The surface had been fully activated surface by weathering. site D was also a fully activated surface, but it consisted of 10.69% sand particles. Sites C and D had the weakest surfaces, with hardness values of 0.5 kg/cm^2 and 0.87 kg/cm^2 (Table 1 and Fig. 1).

The analysis of the particles revealed that the soils of sampling sites A and B contained large agglomerates formed by sticky and powder particles (Fig. 1). The soils from the four sites were dominated by $<63 \mu\text{m}$ particles, and these loose particles provided a sufficient source of sand during wind erosion. The grain size frequency curves for the playa are shown in Fig. 2a). The frequency curves of all of the sites exhibit multiple peaks and similar peak patterns. The particle size mechanical compositions and other parameters of the soil all indicate that the soils in the study area originated from multiple sources [17]. The primary peak of soil A was located at 0.65-7.87 μm , the secondary peak was located at 8.7-52.39 μm . The primary peak of site B was located at 0.53-11.73 μm , the secondary peak was located at 12.96-52.39 μm , and the third peak was located at 105.31-519.61 μm . The primary peak of site C was located at 0.59-8.7 μm , the secondary peak

Table 1. Surface characteristics at the four Chagan Nur Playa sites

	Site A	Site B	Site C	Site D
Soil properties (0-2 cm)				
Clay (%)	52.59	63.81	57.08	49.85
Silt (%)	47.41	31.35	42.61	39.46
Sand (%)	-	4.84	0.31	10.69
USDA texture class	Clay loam	Clay loam	Clay loam	Silt Clay loam
Soil surface characteristics				
Soil moisture (%)	19	7	6	4
Physical clay curls	-	-	✓	✓
Salt crust	✓	✓	-	
Penetrometer resistance (g/cm^2)	3.38	1.69	0.5	0.87
Loose erodible material	-	✓	✓	-
Vegetation				

was located at 9.61-47.41 μm , and the third peak was located at 142.06-285.58 μm . The main peak of site D was located at 0.72-10.62 μm , the secondary peak was located at 11.73-78.08 μm , and the third peak was located at 105.31-574.19 μm . The particle sizes of soils A and C were relatively concentrated and were evenly mixed. The particle sizes of sites B and D were relatively dispersed and the aggregation was poor, indicating that soils B and D were more susceptible to wind erosion. The frequency accumulation curve can reflect the soil transport and dynamic wind characteristics. The steeper the curve is, the better the sorting is, and the stronger and more frequent the wind and sand activity is [17, 18]. The evaluation rate of the accumulation curve of each site is shown in Fig. 2b). The most suspended mass at site B was about 28.01%, and the most creeping mass at site D was about 6.57%. According to the steepness and straightness of the curve, the wind and sand activity was the strongest at sample site B.

Threshold Wind Friction Velocity and Wind Profile

It is generally accepted that the frictional wind velocity occurs when the frictional velocity exceeds the

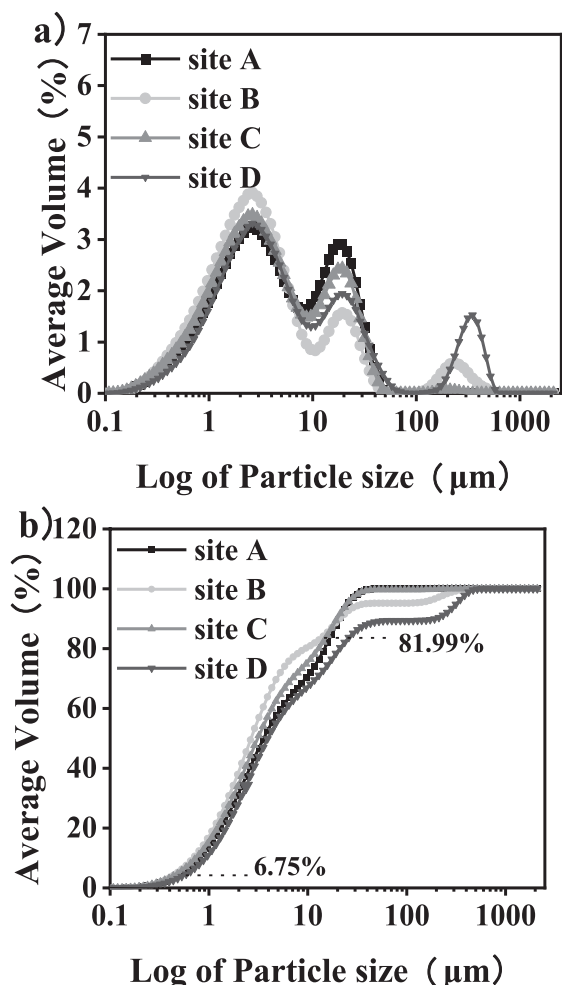


Fig. 2. Soil particle characteristics of the four sample sites.

surface friction threshold, The surface friction threshold velocity is also an important factor in controlling the horizontal sediment flux, and determines the onset of wind erosion [19]. However the soil salt crusts had little effect on the threshold value, and the threshold played a minor role in determining the magnitude of the sediment transport during our observations [20]. The experiment was conducted under neutral stable conditions, so, the variation form of the wind speed profiles of the four sample sites exhibited a logarithmic function relationship, with $R^2 \geq 0.87$ (Table 2). Since the friction velocity at each point was calculated using the wind speeds at different heights, the friction velocity at each point increased with increasing wind speed as follows: $U_d < U_a < U_b < U_c$. The roughness of sites A and B decreased with increasing wind speed. The roughness of sites C and D initially decreased and then increased. The roughness values of the sample sites were similar and the order of the friction velocities was $Z_d < Z_a < Z_b < Z_c$. However, we found that the roughness values of the sites during wind erosion occurring were as follows: $Z_d < Z_c < Z_b < Z_a$.

As can be seen from Fig. 3a), the wind speed changed more with height at site A than at the other three sites. The wind speed at site A changed sharply with height in the range of up to 50 cm, changed slowly above 50 cm, and the wind speed even decreased in the height range of 50-100 cm (Fig. 3b). The wind speed at site B increased sharply in the range of up to 50 cm when the wind speed did not exceed 11.56 m/s at a height of 2 m. When the wind speed exceeded 11.56 m/s, it decreased in the height range of up to 30 cm and increased slowly above 30cm (Fig. 3c). The change in the wind speed site C in the height range of up to 50 cm was slightly larger than that above 50 cm (Fig. 3d). The wind speed at site D changed greatly in the height range of up to 30 cm, and changed slowly above 30cm (Fig. 3e). The above results show that the crust surface may have affected the wind speed below 100 cm, the broken and activated loose surfaces mainly affected the wind speed below 50 cm, and the sandy surface mainly affected the wind speed below 30 cm.

Sediment Mass Flux Due to Wind Erosion

The largest sediment fluxes were recorded at site B (627.55 g) and site D (587.43 g), the smallest sediment flux was recorded at site A (30.51 g), and the sediment flux recorded at site C was medium (520.79 g) (Fig. 4a). This indicates that the sand transport of the crust surfaces was lower than that of the loose surface. Fig. 4b) compares the sediment transport rates at height of 4-10 cm, 10-20 cm, 20-30 cm, and 30-40 cm. It was found that if the 0-4 cm sediment at sites B and C was not lost, a larger sediment flux was recorded. The sediment flux at site C could exceed that at site D, and the sediment transport at a height of 50 cm was greater at site C more than at the other sites.

Table 2. Roughness and friction speed of the sample plot during the experimental test.

Sites	Mean Wind speed (m/s) at 2 m	<i>a</i>	<i>b</i>	<i>u</i> * (m/s)	<i>z</i> ₀ (cm)	<i>R</i> ²
A	9.83	8.61	3.76	1.50	0.10	0.98
	10.28	9.55	3.05	1.22	0.04	0.91
	11.34	10.66	3.18	1.27	0.04	0.84
	12.64	11.90	3.37	1.35	0.03	0.83
	13.86	13.03	3.60	1.44	0.03	0.8
Average value	11.59	10.75	3.39	1.36	0.05	0.87
B	9.41	8.63	3.30	1.32	0.07	0.96
	10.73	9.81	3.64	1.46	0.07	0.95
	11.56	10.55	3.60	1.44	0.05	0.93
	12.52	11.42	3.67	1.47	0.04	0.87
	13.37	12.15	3.73	1.49	0.04	0.78
Average value	11.52	10.51	3.59	1.44	0.06	0.90
C	9.28	8.21	3.06	1.22	0.07	0.98
	11.05	10.1	3.46	1.38	0.05	0.98
	11.51	10.28	3.53	1.41	0.05	0.98
	12.64	11.36	3.91	1.56	0.05	0.98
	13.96	12.32	4.58	1.83	0.07	0.98
Average value	11.68	10.45	3.71	1.48	0.06	0.98
D	8.66	7.96	2.36	0.94	0.03	0.95
	9.55	8.71	2.32	0.93	0.02	0.97
	10.76	9.78	2.54	1.02	0.02	0.97
	12.11	10.95	2.86	1.14	0.02	0.97
	13.86	12.4	3.43	1.37	0.03	0.95
Average value	10.99	9.96	2.70	1.08	0.03	0.96

Commonly the sediment flux near the surface was significantly greater than the amount of sediment sampled from the surface. This finding was confirmed by the good fit of the data used to calculate the vertically integrated sediment mass fluxes with a linear function for site A ($R^2 = 0.99$), a power function for site B ($R^2 = 0.96$), and exponential functions for sites C ($R^2 = 0.96$) and D ($R^2 = 0.93$) (Fig. 5).

Particle Size Distribution of Sediment Flux

Fig. 6 shows the changes in the regulation of the playa sediment particle size in the vertical direction. For all of the sites, based on the Udden-Wentworth scale, silt and clay were the predominant particle sizes in the horizontal sediment flux. An interesting phenomenon was observed: the quantity of material with a particle size of greater than 63 μm in each height interval at the four sampling sites was very small. Based on the results for the dust storm events, the wind erosion of >63 μm particles was the greatest at site A (28.51%), followed by site D (11.1%), and site C (9.06%), and it was the lowest at site B (3.67%). The number of >63 μm particles increased significantly at 8-10 cm and then

returned to the original stable content at 22-26 cm for all of the sites. The content of >63 μm particles above a height of 22 cm seemed to increase, but the increase was not obvious. The quantities of the salinized particles of different sizes in each sample site were less than 2.5 μm >2.5-10 μm >10-63 μm >larger than 63 μm , except for site A where the order was larger than 63 μm >2.5-10 μm >10-63 μm . As can be seen from Table 1, the surface soil at site A was entirely composed of <63 μm clay and silt particles, whereas during the sediment transport, 28.51% of the particles were >63 μm , indicating that the supply of sand and dust at the crust surface was much lower.

Particle Size Parameters of Sediment Flux

The mean particle size, sorting coefficient, skewness, and kurtosis within the height range of up to 50 cm in the sand collector are shown in Fig. 7. The mean particle size (ϕ) value at site A was mainly 5-7, which is classified as silt. It decreased with height up to 10 cm and remained basically unchanged above 10 cm height. The mean particle sizes at sites B, C, D were primarily 7-9, which is classified as clay. The mean

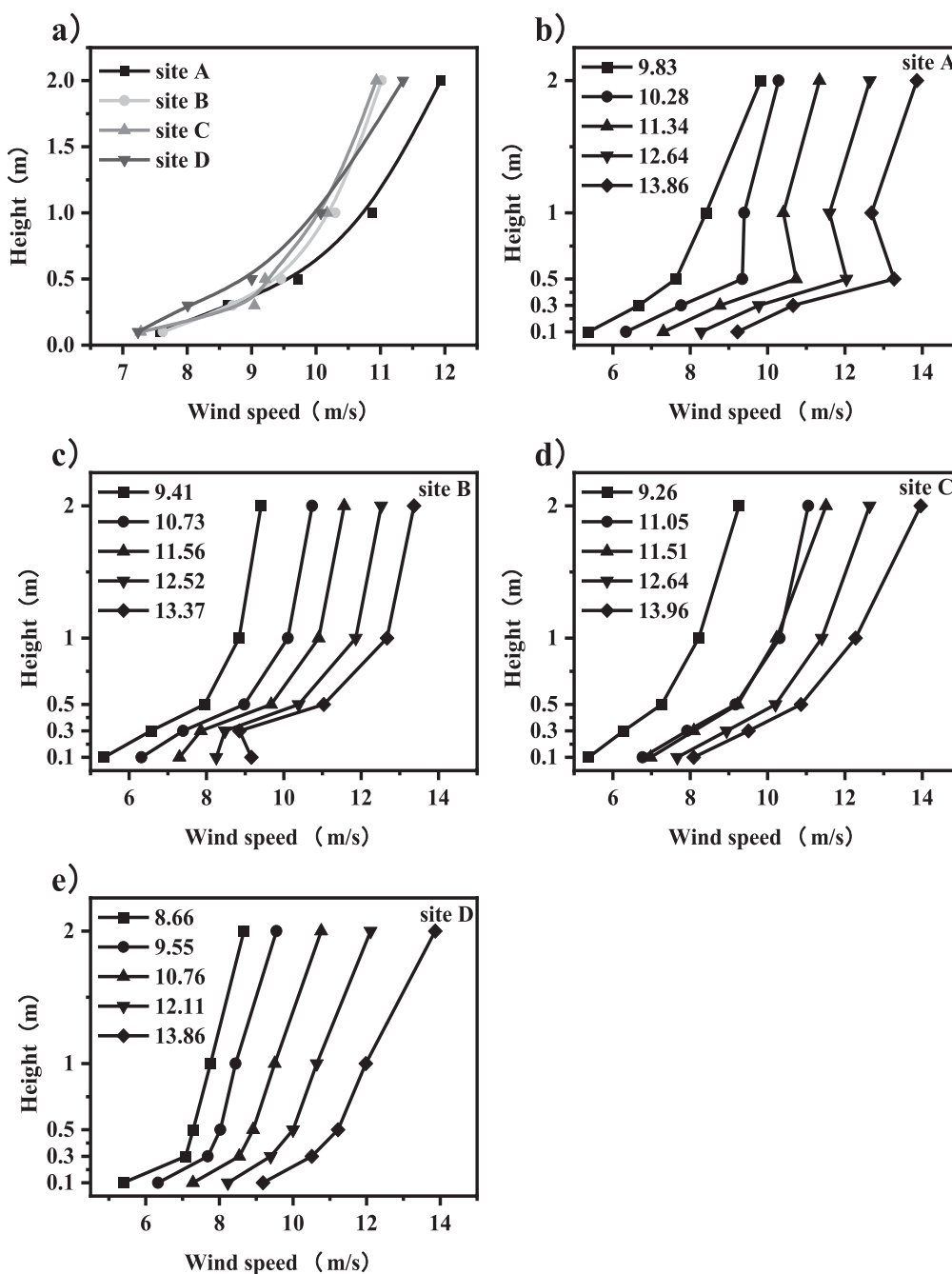


Fig. 3. Wind speeds at various heights above the surface of four study sites.

particle size decreased with a height 22 cm. The mean particle size at all heights was as follow: B (8.17)>C (7.74)>D (7.41)>A (6.30). The sorting value at each sample site was 1-4, and the sorting was relatively poor. The sorting at site A was the worst, indicating that the particles transported by wind erosion were chaotic, but more uniform. The skewness was negative at all of the sites. The skewness of site A was the smallest, and the skewness increased with height; while it decreased with height at sites B, C, and D were opposite. The kurtosis values revealed that site A was platykurtic, while the other three sites were mesokurtic to leptokurtic. The above particle size parameters indicate that the wind erosion species at site A were mixed with foreign

substances, while the wind erosion species at sites B, C, and D mainly came from the salinization of surface particles, and the particles transported via wind erosion became finer with increasing height.

Discussion

Under natural conditions in the field, the factors controlling the flow of wind and sand mainly include wind speed, sand source abundance, and surface stability. The playa consisted entirely of bare land without any vegetation cover during the wind and sand prevalence measurement, so the effect on the

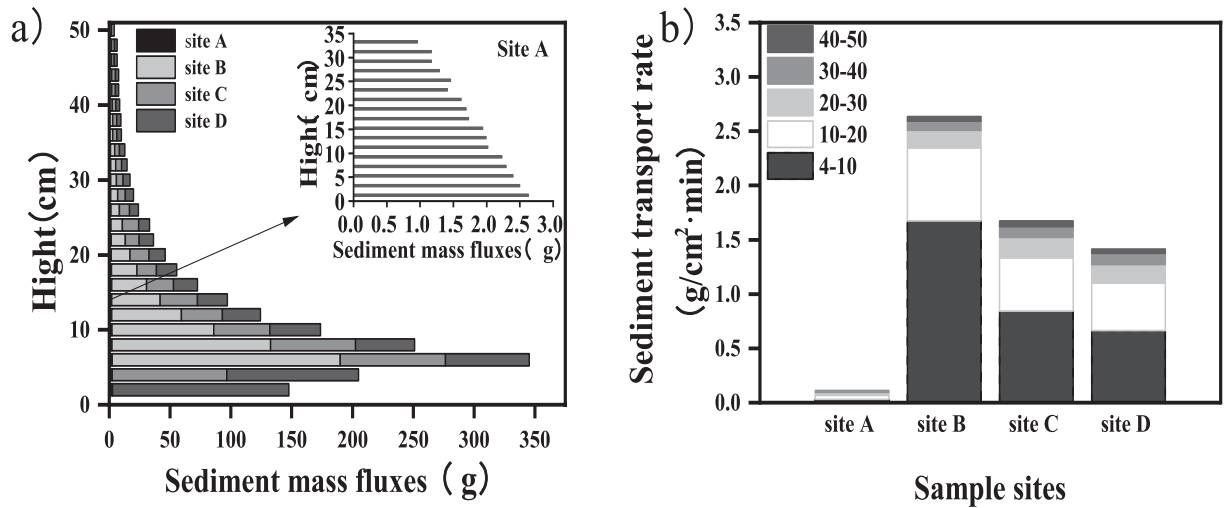


Fig. 4. Variation of horizontal sediment fluxes with height at 4 sites.

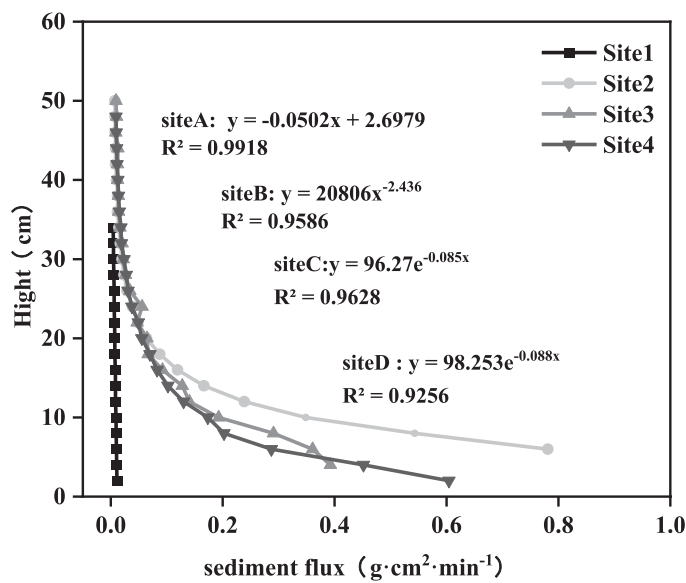


Fig. 5. Functional relationship between the aeolian sediment flux and height at the four observation sites.

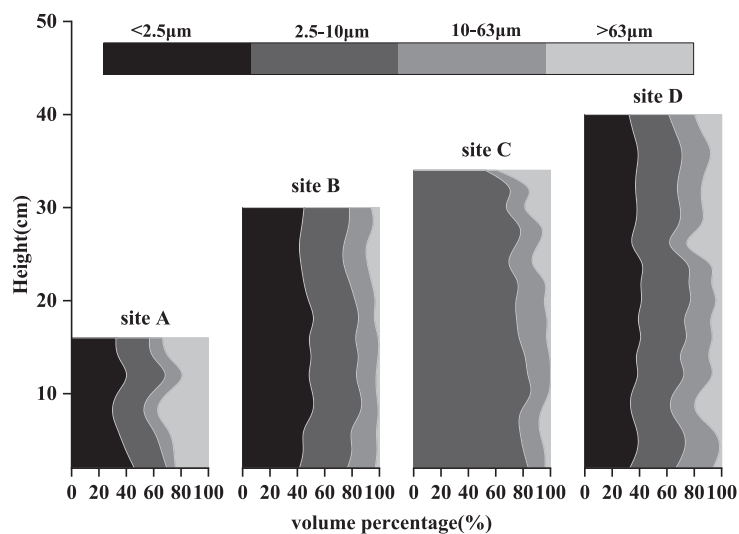


Fig. 6. Distribution characteristics of the soil grains at various heights for all of the sites.

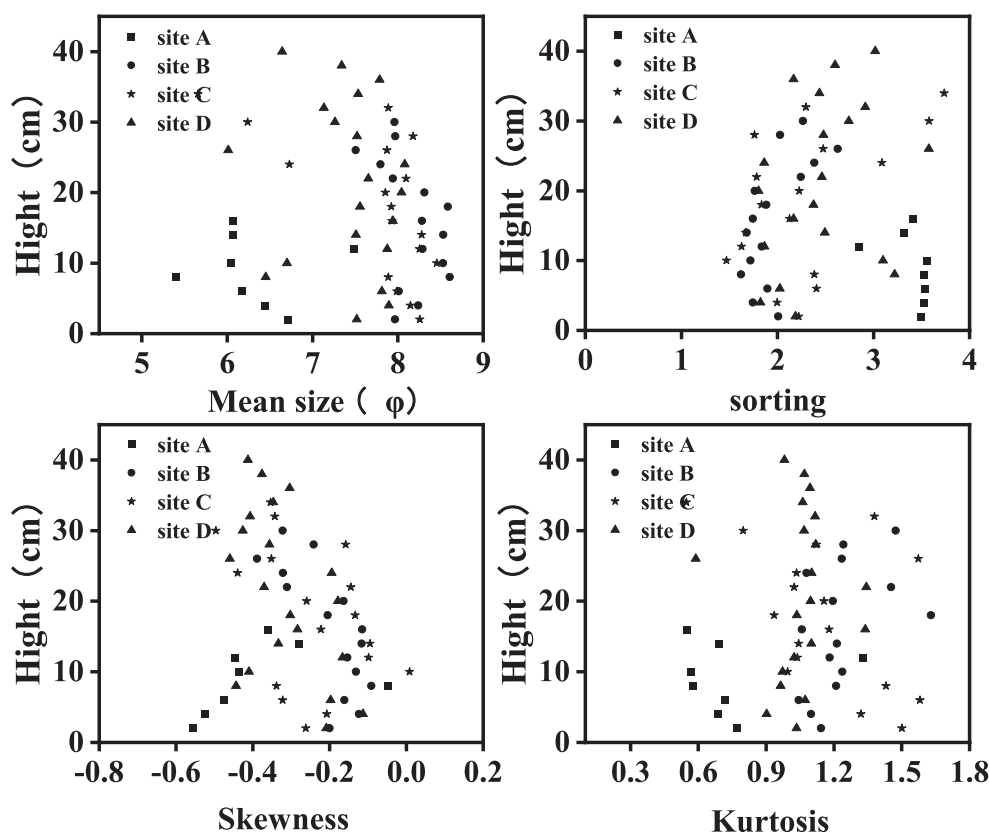


Fig. 7. Distribution characteristics of the soil particle size parameters at various heights for all of the sites.

sand flow due to wind was only controlled by the wind characteristics of the surface soils and the characteristics of the ground surface [21]. We discovered that soil moisture is the key factor in surface crust formation. The soil particles in the study area were generally fine and clay particles. The crust formed in the wetland at the beginning of the drying process had a strong resistance to wind erosion, but the surface was gradually weakened by weathering and abrasion. In particular, particles carried by high-energy wind impacted the surface, and the crusts were destroyed due to long-term exposure to such impacts, so the surface formed more loose particles in the low wind energy environment. The wind erosion of the surface was further strengthened, and a large number of dust particles was released [22, 23]. Finally, the surface was fully activated (Fig. 8). Numerous studies have demonstrated that soils with a low organic matter content and low fine particle content are more vulnerable to wind erosion [24]. Shahabinejad et al. [10] reported a positive exponential relationship between the sand content and wind erosion; whereas, clay and silt particles are inversely correlated with wind erosion. Similarly Colazo et al. [25] believed that the soil loss rate due to wind and the soil clay content are negatively correlated. A height clay content can reduce wind erosion because the existence of clay particles enhances the binding force of the soil and clay [26]. Therefore, it can be concluded that the size of the soil aggregates is very important in surface erosion and

controls the horizontal migration of sediments. During the observation period, it was observed that it was easy for the aggregates in the playa to become completely dispersed particles after drying and to be eroded by wind. The primary particle size and wind erosion rate of the soil may be related to other hidden characteristics of the soil, especially the secondary particles (soil aggregates) formed [26]. The soils at all of the sites were mainly clay and silt and easily formed aggregates and crusts of secondary particles when exposed to water. As the inter-aggregate cohesion of the particles increase, the wind erosion resistance of the surface increases [27]. However, the study area has a semi-arid climate and has been disturbed by the monsoon for a long time. In addition, the ground surface is dry and contains an abundance of salt, soil aggregates, and other erosion-resistant materials, and the aggregate forces among particles have been reduced by soil moisture evaporation [21]. Thus, the stable surface structures have been destroyed, causing the crust to be quickly eroded and broken up and producing a large amount of dust [28, 29]. Near-surface wind speeds and dust emissions vary among land use types and are influenced by gravel, vegetation, the silt and clay content, and crusts [30, 31]. Deserts are widespread but contain only <5% clay and silt. Such sediments are transports over limited distances and are not a major source of dust [23, 32]. The Gobi Desert was found to contain mainly 63-125 μm particles and to be finer than the average desert particle size

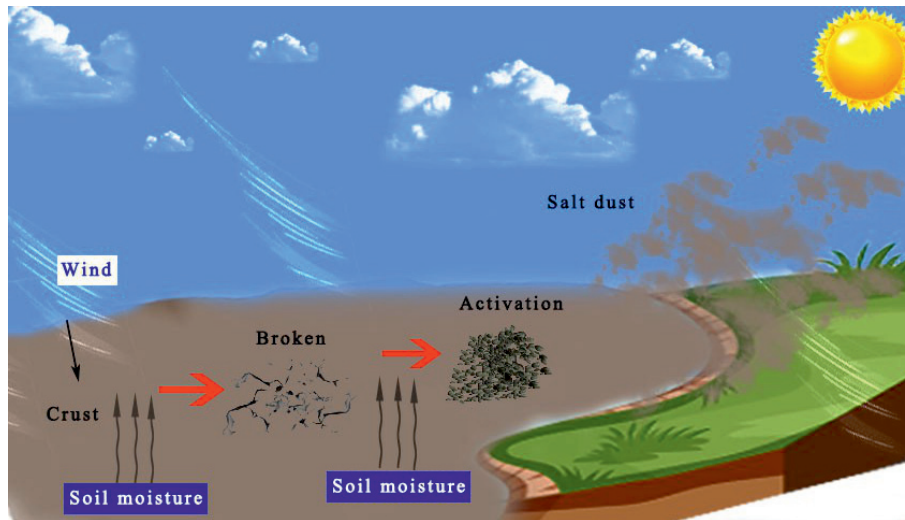


Fig. 8. Formation and activation processes of the playa surface.

(125-250 μm), leading to the generation of more dust [30]. Gravel contributes to dust reduction at certain cover levels, and dust emissions are constant when the gravel cover exceeds 50% [33]. The wind speed at site A (Fig. 2) was significantly greater than those of the other three sites with increasing height. Because gravel, vegetation, and soil crusts can protect the surface by increasing the cohesion of the surface and as the roughness, the threshold shear velocity of the crust increases [34], and the wind passing through the playa activation surface contains a large number of salt dust particles, which collide with each other, weakening the kinetic energy of the particles and reducing the variation in the wind velocity with height [35]. The larger soil aggregates in the initial stage of crust crushing and activation of the playa increased the aerodynamic roughness and the resistance to wind erosion [36]. In addition, the erodible particles on the surface greatly increase with creep or overrun on the ground, and the kinetic energy is consumed. The friction speed and roughness values also demonstrated that the changes in the wind speed at the four sites were consistent with this principle. However, our results suggested that for the surface of the playa, the frictional velocity and roughness may not always play a dominant role in determining the magnitude of the horizontal mass flux. In a limited sediment supply system, the roughness plays a secondary role in determining sediment flux [20, 37]. The wind-sand flow allows the crust to overcome the resistance to do work. This causes the ground surface of the to produce a large number of erodible particles [38]. The particles at sites C and D had been activated through wind and sand grinding to produce more fine particles ($<63 \mu\text{m}$), which could migrate directly upward and can migrate farther relative to particles from deserts (125-250 μm) and the Gobi desert (63-125 μm) [39, 40]. For the wind erosion samples we collected, the particle size of the wind erosion was greater above a height of 20 cm than

below 20 cm. This was presumably because the wind erosion flow carried a certain amount of coarser sand on its entry, but the $<63 \mu\text{m}$ sand was much larger than the sand carried in the wind erosion flow in the height up to 20 cm near the surface, resulting in a relative increase in the coarse particle content of the wind erosion particles above a height of 20 cm. In addition, the particle size parameters also revealed that the sorting performance of the wind erosion became poorer from site A to site D, the skewness became extremely negative, and the kurtosis changed from wide and flat to sharp and narrow, which is also consistent with the principle.

Conclusions

In this study, the natural wind conditions at four field sites were explored to characterize the salt dust emissions from a crusted activated playa surface in a typical steppe, including four types of soil surfaces in a clay-rich playa. We discovered that the salinized particles on the surface of the study area were extremely fine clay and powder particles, accounting for about $\geq 90\%$, while the sand particles accounted $<11\%$; from the lake's center to the shore, the salinized particles gradually became coarser. The surface at the lake's center was a crust with salt frost. Moreover, with decreasing distance from the shore, the surface transitioned to broken crusts, then to a loosely activated surface, and finally to an activated sandy surface. The wind speed, friction velocity, and roughness decreased in the following order: sandy surface $<$ crust $<$ broken crust $<$ activated surface. The sand transport was concentrated within the height of up to 30 cm height for all four types of surfaces. At site A, the sand transport exhibited a linear function with height ($R^2 = 0.99$), which was visibly different from the exponential function at site B as an ($R^2 = 0.96$) and the Power functions at sites C, and D ($R^2 = 0.96$, $R^2 = 0.93$). Site A had the

lowest total sand transport, and the sand transport at the activated sites (C, and D) was slightly lower than that for the broken crust, but the sediment transport rate of the activated surface above a height of 20 cm exceeded that of the broken crust surface. The collected wind erosion materials revealed that the salt dust particles were generally fine. In addition, the mean particle size at site A decreased within the height of up to 10 cm and remained basically unchanged above 10 cm. At sites B, C, and D, the mean particle size increased above 22 cm. The skewness values of all of the sites were negative, and the kurtosis values showed that from sites A-D the kurtosis changed from platykurtic to mesokurtic to leptokurtic. As such, lakes in typical steppes may undergo a similar process, continuously releasing a large number of fine particles and becoming a source of dust storms.

Acknowledgments

This research was supported by the National Natural Science Foundation of China (42067015), and the Natural Science Foundation of Inner Mongolia Autonomous Region (2020MS03038), and the Desert Ecosystem Conservation and Restoration Innovation Team, and Improvement Innovation Team of Desertification Control (BR22-13-03).

Declaration of Interest Statement

The authors declare no competing interests. This manuscript, entitled “Dust release during playa activation in a semiarid typical steppe”, is original and has not been previously published.

References

- FRIE A.L., GARRISON A.C., SCHAEFER M.V., BATES S.M., BOTTHOFF J., MALTZ M., YING S.C., LYONS T., ALLEN M.F., ARONSON E., BAHREINI R. Dust Sources in the Salton Sea Basin: A Clear Case of an Anthropogenically Impacted Dust Budget. *Environ Sci Technol*, **53**, 9378, **2019**.
- VARGA G., UJVARI G., KOVACS J. Spatiotemporal patterns of Saharan dust outbreaks in the Mediterranean Basin. *Aeolian Research*, **15**, 151, **2014**.
- MOTAGHI F.A., HAMZEHPUR N., ABASIYAN S.M.A., RAHMATI M. The wind erodibility in the newly emerged surfaces of Urmia Playa Lake and adjacent agricultural lands and its determining factors. *Catena*, **194**, 104675, **2020**.
- MIDDLETON N.J. Desert dust hazards: A global review. *Aeolian Research*, **24**, 53, **2017**.
- ZIYAEE A., KARIMI A., HIRNAS D.R., KEHL M., LAKZIAN A., KHADEMI H., MECHEM D.B. Spatial and temporal variations of airborne dust fallout in Khorasan Razavi Province, Northeastern Iran. *Geoderma*, **326**, 42, **2018**.
- WANG J., DING J., LI G., LIANG J., YU D., AISHAN T., ZHANG F., YANG J., ABULIMITI A., LIU J. Dynamic detection of water surface area of Ebinur Lake using multi-source satellite data (Landsat and Sentinel-1A) and its responses to changing environment. *Catena*, **177**, 189, **2019**.
- LI X., CHENG H., TAN L., BAN F., SINHA A., DUAN W., LI H., ZHANG H., NING Y., KATHAYAT G., EDWARDS R.L. The East Asian summer monsoon variability over the last 145 years inferred from the Shihua Cave record, North China. *Sci Rep*, **7**, 7078, **2017**.
- TADA R., ZHENG H.B., CLIFT P.D. Evolution and variability of the Asian monsoon and its potential linkage with uplift of the Himalaya and Tibetan Plateau. *Progress In Earth And Planetary Science*, **3**, 4, **2016**.
- LI G.Q., WANG Z., ZHAO W.W., JIN, M., WANG X.Y., TAO S.X., CHEN C.Z., CAO X.Y., ZHANG Y.N., YANG H., MADSEN D. Quantitative precipitation reconstructions from Chagan Nur revealed lag response of East Asian summer monsoon precipitation to summer insolation during the Holocene in arid northern China. *Quaternary Science Reviews*, **239**, 106365, **2020**.
- SHAHABINEJAD N., MAHMOODABADI M., JALALIAN A., CHAVOSHI E. The fractionation of soil aggregates associated with primary particles influencing wind erosion rates in arid to semiarid environments. *Geoderma*, **356**, 113936, **2019**.
- PI H., SHARRATT B. Threshold Friction Velocity Influenced by the Crust Cover of Soils in the Columbia Plateau. *Soil Science Society of America Journal*, **83**, 232, **2019**.
- DYER K.R. VELOCITY PROFILES OVER A RIPPLED BED AND THE THRESHOLD OF MOVEMENT OF SAND. *Estuarine And Coastal Marine Science*, **10**, 181, **1980**.
- WIGGS G.F., LIVINGSTONE I., THOMAS D.S., BULLARD, J.E.J.E.S.P., LANDFORMS. Airflow and roughness characteristics over partially vegetated linear dunes in the southwest Kalahari Desert. **21**, 19, **1996**.
- PI H., HUGGINS D.R., SHARRATT B. Threshold friction velocities influenced by standing crop residue in the inland Pacific Northwest, USA. *Land Degradation & Development*, **31**, 2356, **2020**.
- CHEPIL W., WOODRUFF N.J.A.J.O.S. Sedimentary characteristics of dust storms; Part II, Visibility and dust concentration. **255**, 104, **1957**.
- FOLKRL W.J.J. A study in the significance of grain size parameters. **27**, , **1957**.
- YAN B., ZHANG Y., ZANG S., CHEN Q., SUN L. Distributions of Particle Sizes in Black Soil and Their Environmental Significance in Northeast China. *Sustainability*, **13**, 3706, **2021**.
- ALBADI H., BOLAND J., BRUCE D., WEDDING B. Estimating effective dust particle size from satellite observations. *Remote Sensing Applications: Society and Environment*, **11**, 186, **2018**.
- PIERRE C., BERGAMETTI G., MARTICORENA B., ABDOURHAMANETOURÉ A., RAJOT J.L., KERGOAT, L. Modeling wind erosion flux and its seasonality from a cultivated sahelian surface: A case study in Niger. *Catena*, **122**, 61, **2014**.
- WEBB N.P., GALLOZA M.S., ZOBECK T.M., HERRICK J.E. Threshold wind velocity dynamics as a driver of aeolian sediment mass flux. *Aeolian Research*, **20**, 45, **2016**.

21. CHENG H., LIU C., LI J., ZOU X., LIU B., KANG L., FANG Y. Wind erosion mass variability with sand bed in a wind tunnel. *Soil and Tillage Research*, **165**, 181, **2017**.
22. KHEIRFAM H., ASADZADEH F. Stabilizing sand from dried-up lakebeds against wind erosion by accelerating biological soil crust development. *European Journal of Soil Biology*, **98**, 103189, **2020**.
23. FATTAHI S.M., SOROUSH A., HUANG N., ZHANG J., JODARI ABBASI S., YU Y. A framework for predicting abrasion rupture of crusts in wind erosion. *Earth Surface Processes and Landforms*, **46**, 2565, **2021**.
24. ZHANG C., WANG X., ZOU X., TIAN J., LIU B., LI J., KANG L., CHEN H., WU Y. Estimation of surface shear strength of undisturbed soils in the eastern part of northern China's wind erosion area. *Soil and Tillage Research*, **178**, 1, **2018**.
25. COLAZO J.C., BUSCHIAZZO D.E. Soil dry aggregate stability and wind erodible fraction in a semiarid environment of Argentina. *Geoderma*, **159**, 228, **2010**.
26. FEIZI Z., AYOUBI S., MOSADDEGHI M.R., BESALATPOUR A.A., ZERAATPISHEH M., RODRIGO-COMINO J. A wind tunnel experiment to investigate the effect of polyvinyl acetate, biochar, and bentonite on wind erosion control. *Archives of Agronomy and Soil Science*, **65**, 1049, **2018**.
27. AYOUBI S., MOKHTARI J., MOSADDEGHI M.R., ZERAATPISHEH, M. Erodibility of calcareous soils as influenced by land use and intrinsic soil properties in a semiarid region of central Iran. *Environ Monit Assess*, **190**, 192, **2018**.
28. SWEENEY M.R., ZLOTNIK V.A., JOECKEL R.M., STOUT J.E. Geomorphic and hydrologic controls of dust emissions during drought from Yellow Lake playa, West Texas, USA. *Journal of Arid Environments*, **133**, 37, **2016**.
29. DING X., XU G., KIZIL M., ZHOU W., GUO X. Lignosulfonate Treating Bauxite Residue Dust Pollution: Enhancement of Mechanical Properties and Wind Erosion Behavior. *Water, Air, & Soil Pollution*, **229**, 214, **2018**.
30. ZHANG Z., DONG Z., WU G. Field observations of sand transport over the crest of a transverse dune in northwestern China Tengger Desert. *Soil and Tillage Research*, **166**, 67, **2017**.
31. CUI M., LU H., WIGGS G.F.S., ETYEMEZHIAN V., SWEENEY M.R., XU Z. Quantifying the effect of geomorphology on aeolian dust emission potential in northern China. *Earth Surface Processes and Landforms*, **44**, 2872, **2019**.
32. SWET N., KOK J.F., HUANG Y., YIZHAQ H., KATRA I. Low Dust Generation Potential From Active Sand Grains by Wind Abrasion. *Journal of Geophysical Research: Earth Surface*, **125**, e2020JF005545, **2020**.
33. TAN L., ZHANG W., QU J., ZHANG K., AN Z., WANG X. Aeolian sand transport over gobi with different gravel coverages under limited sand supply: A mobile wind tunnel investigation. *Aeolian Research*, **11**, 67, **2013**.
34. ZHANG Z., ZHANG Y., PAN K. Characteristics of Aeolian sediments transported above a gobi surface. *Atmos. Chem. Phys. Discuss.*, **2022**, 1, **2022**.
35. LIU B., WANG Z., NIU B., QU J. Large scale sand saltation over hard surface: a controlled experiment in still air. *Journal of Arid Land*, **13**, 599, **2021**.
36. KHEIRABADI H., MAHMOODABADI M., JALALI V., NAGHAVI H. Sediment flux, wind erosion and net erosion influenced by soil bed length, wind velocity and aggregate size distribution. *Geoderma*, **323**, 22, **2018**.
37. O'BRIEN P., MCKENNA NEUMAN C. A wind tunnel study of particle kinematics during crust rupture and erosion. *Geomorphology*, **173-174**, 149, **2012**.
38. VAN PELT R.S., TATARKO J., GILL T.E., CHANG C., LI J., EIBEDINGIL I.G., MENDEZ M. Dust emission source characterization for visibility hazard assessment on Lordsburg Playa in Southwestern New Mexico, USA. *Geoenvironmental Disasters*, **7**, 34, **2020**.
39. WANG X., ZHANG C. Field observations of sand flux and dust emission above a gobi desert surface. *Journal of Soils and Sediments*, **21**, 1815, **2021**.
40. SWEENEY M.R., FORMAN S.L., MCDONALD E.V. Contemporary and future dust sources and emission fluxes from gypsum- and quartz-dominated eolian systems, New Mexico and Texas, USA. *Geology*, **50**, 356, **2021**.